HHS Public Access

Author manuscript

Cancer Res. Author manuscript; available in PMC 2016 April 15.

Published in final edited form as:

Cancer Res. 2015 April 15; 75(8): 1657–1667. doi:10.1158/0008-5472.CAN-14-2061.

MyD88-dependent signaling decreases the anti-tumor efficacy of epidermal growth factor receptor inhibition in head and neck cancer cells

Adam T. Koch[1,5], **Laurie Love-Homan**[1,5], **Madelyn Espinosa-Cotton**[2,5], **Aditya Stanam**[3,5], and **Andrean L. Simons**[1,2,3,4,5]

[1]Department of Pathology, The University of Iowa, Iowa City, IA

[2]Free Radical and Radiation Biology Program, Department of Radiation Oncology, The University of Iowa, Iowa City, IA

[3]Interdisciplinary Human Toxicology Program, The University of Iowa, Iowa City, IA

[4]Holden Comprehensive Cancer Center, The University of Iowa, Iowa City, IA

[5]Roy J. and Lucille A. Carver College of Medicine, The University of Iowa, Iowa City, IA

Abstract

Epidermal growth factor receptor (EGFR) is upregulated in the majority of head and neck squamous cell carcinomas (HNSCC). However many HNSCC patients respond poorly to the EGFR inhibitors (EGFRIs) cetuximab and erlotinib despite tumor expression of EGFR. Gene expression analysis of erlotinib-treated HNSCC cells revealed an upregulation of genes involved in MyD88-dependent signaling compared to their respective vehicle-treated cell lines. We therefore investigated if MyD88-dependent signaling may reduce the anti-tumor efficacy of EGFRIs in HNSCC. Erlotinib significantly upregulated interleukin-6 (IL-6) secretion in HNSCC cell lines which our laboratory previously reported to result in reduced drug efficacy. Suppression of MyD88 expression blocked erlotinib-induced IL-6 secretion *in vitro* and increased the anti-tumor activity of erlotinib *in vivo*. There was little evidence of toll-like receptor or interleukin-18 receptor involvement in erlotinib-induced IL-6 secretion. However, suppression of interleukin-1 receptor (IL-1R) signaling significantly reduced erlotinib-induced IL-6 production. A time-dependent increase of IL-1 alpha (IL-1α) but not IL-1 beta (IL-1β) was observed in response to erlotinib treatment and IL-1α blockade significantly increased the anti-tumor activity of erlotinib and cetuximab *in vivo*. A pan-caspase inhibitor reduced erlotinib-induced IL-1α secretion suggesting that IL-1α was released due to cell death. Human HNSCC tumors showed higher IL-1α mRNA levels compared to matched normal tissue, and IL-1α was found to be negatively correlated with survival in HNSCC patients. Overall, the IL-1α/IL-1R/MYD88/IL-6 pathway may be responsible for the reduced anti-tumor efficacy of erlotinib and other EGFRIs; and blockade of IL-1 signaling may improve the efficacy of EGFRIs in the treatment of HNSCC.

*Corresponding author: Andrean L. Simons, PhD, Assistant Professor, Department of Pathology, 1161 Medical Laboratories, University of Iowa, Iowa City, IA 52242, Phone: (319) 384-4450, Fax: (319) 335-8453, andrean-simons@uiowa.edu.

The authors have no conflict of interest.

Keywords

EGFR; Erlotinib; MyD88; IL-1α; IL-1R; TLR; inflammation; HNSCC

Introduction

The epidermal growth factor receptor (EGFR) is a receptor tyrosine kinase that activates numerous pro-survival pathways including Akt and STAT3 signaling pathways (1). Given that EGFR signaling is upregulated in many cancers especially head and neck squamous cell carcinoma (HNSCC), several drugs that target EGFR have been developed and approved for cancer therapy such as monoclonal antibodies that block the extracellular ligand binding domain (e.g. cetuximab, panitumumab) and small molecule tyrosine kinase inhibitors (TKIs) that prevent activation of the cytoplasmic tyrosine kinase domain (e.g. gefitinib, erlotinib) (1). To date, only cetuximab is FDA approved for use in HNSCC, however it should be noted that response rates to cetuximab as a single agent are quite low (13%) and of limited duration (2–3 months). Similarly, low response rates (4–11%) have been observed in clinical trials with HNSCC patients treated with gefitinib and erlotinib (2–5). Many different mechanisms (e.g. existing/acquired mutations and alternative signaling pathways) have been proposed that may reduce patient response to EGFRIs, but this knowledge has not improved survival rates for HNSCC patients to date (6–9).

Previous studies in our laboratory observed a significant upregulation in IL-6 expression in HNSCC cell lines treated with EGFRIs (10). IL-6 is a pleotropic cytokine with a wide range of biological activities and is well known for its role in inflammation, tumor progression and chemoresistance in HNSCC (11–14). We additionally demonstrated the ability of IL-6 signaling to protect HNSCC against erlotinib (ERL) treatment *in vitro* and *in vivo* (10) supporting prior reports showing that IL-6 may be involved in resistance to EGFRIs (15–18).

A well-established mechanism of IL-6 production involves the cytosolic adaptor protein myeloid differentiation primary response gene 88 (MyD88), which acts through intermediaries to induce nuclear factor kappa-light-chain-enhancer of activated B cells (NFκB) activation (19). MyD88 is required for the activity of members of the Toll/Interleukin-1 receptor (TIR) superfamily which include Toll-like Receptors (TLRs), the Interleukin-1 Receptor (IL-1R), and the IL-18 Receptor (IL-18R) (19). Activation of these receptors lead to the recruitment of MyD88 via its TIR domain resulting in NFkB activation and expression of pro-inflammatory cytokines including IL-6 (19). Here we show that EGFR inhibition using ERL activates the IL-1α/IL-1R/MyD88/IL-6 signaling pathway and this pathway may serve as a novel mechanism responsible for the poor long-term anti-tumor efficacy of EGFRIs in HNSCC therapy.

Materials and Methods

Cells and Culture Conditions

Cal-27 and FaDu human head and neck squamous carcinoma (HNSCC) cells were obtained from the American Type Culture Collection (ATCC, Manassas, VA). SQ20B HNSCC cells (20) were a gift from Dr. Anjali Gupta (Department of Radiation Oncology, The University of Iowa). All HNSCC cell lines are EGFR positive and are sensitive to EGFR inhibitors. All cell lines were authenticated by the ATCC for viability (before freezing and after thawing), growth, morphology and isoenzymology. Cells were stored according to the supplier's instructions and used over a course of no more than 3 months after resuscitation of frozen aliquots. Cultures were maintained in 5% CO_2 and air humidified in a 37°C incubator.

In Vitro Drug Treatment

Erlotinib (ERL; Tarceva), anakinra (ANA; Kineret) and N-acetyl cysteine (NAC; Acetadote) were obtained from the inpatient pharmacy at the University of Iowa Hospitals and Clinics. Drugs were added to cells at final concentrations of 5 μM ERL, 10 ng/mL or 50 ng/mL ANA and 20 mM NAC. Human IgG and dimethyl sulfoximine (DMSO) were used as controls and were obtained from Sigma Aldrich. Pegylated catalase (CAT; Sigma Aldrich) was used at a final concentration of 100 U/mL. Human IL-1α, IL-1β, and IL-18Rα neutralizing antibodies were obtained from R&D Systems and were used at a concentration of 0.5 μg/mL. Recombinant human IL-1α was obtained from Life Technologies and administered at a concentration of 1 ng/mL. Ac-Y-VAD-cho (CalBioChem) was suspended in DMSO and used at 5 μM. Z-VAD-fmk (Promega) was diluted in DMSO and used at 20 μM. TLR agonists were used at the following concentrations: Pam3CSK4 (200ng/mL), FSL-1 (100ng/mL), Poly I:C (20μg/mL), LPS (200ng/mL), Flagellin (200ng/mL), Gardiquimod (1μg/mL), CL075 (1μg/mL), and *E. coli* DNA (1 μg/mL). All TLR agonists were obtained from InvivoGen. The required volume of each drug was added directly to complete cell culture media on cells to achieve the indicated final concentrations.

Microarray Analyses

Gene expression analysis of HNSCC cells treated with DMSO or erlotinib (5 μM, 48 h) has been described previously (GeneBank accession no. GSE45891 (10)). Downstream pathway, network, process and disease analyses of the resultant gene expression data for all cell lines (n=3 experiments per cell line) was carried out using MetacoreTM (GeneGo) using a threshold of +1.3 and a p-value of 0.05. Enrichment analysis of the resultant gene expression profiles of SQ20B and Cal-27 HNSCC cells exposed to ERL versus DMSO was performed by mapping gene IDs from the resultant dataset onto gene IDs in built-in functional ontologies which include cellular/molecular process networks, disease biomarker networks, canonical pathway maps and metabolic networks.

Real-Time quantitative PCR

Total RNA was extracted from cells after indicated time points using RNeasy Plus mini kit (Qiagen). Conversion of RNA into cDNA was accomplished with the iScript cDNA synthesis kit (Bio-Rad) and a thermocycler with the following conditions: 5 minutes at

25°C, 30 minutes at 42°C, and 5 minutes at 85°C. Subsequent RTPCR analysis was performed in a 96-well optical plate with each well containing 6μL of cDNA, 7.5 μL of SyBr Green Universal SuperMix (Bio-Rad), and 1.5μL of oligonucleotide primers (sense and antisense; 4μM) for a total reaction volume of 15μL. Oligonucleotide primers for human genes were obtained from IDT (Iowa City, IA) and are as listed in Supplementary Table I. RTPCR was performed on ABI PRISM Sequence Detection System (model 7000, Applied Biosystems) with the following protocol: 95°C for 15 seconds (denaturing) and 60°C for 60 seconds (annealing), repeated for 40 cycles. Threshold cycle (CT) values for analyzed genes (in duplicate) were normalized as compared to GAPDH (cell lines) or 18S (human samples) CT values. Relative abundance was calculated as 0.5^(ΔCT), with ΔCT being the CT value of the analyzed gene minus the CT value of the reference gene (GAPDH or 18S).

Western blot analysis

Cell lysates were standardized for protein content, resolved on 4%–12% SDS polyacrylamide gels, and blotted onto nitrocellulose membranes. Membranes were probed with rabbit anti-MyD88 (1:500, Cell Signaling), anti-IL-1R1 (1:500, Santa Cruz), anti-beta-actin (1:5000, Thermo Scientific). Antibody binding was detected by using an ECL Chemiluminescence Kit (Amersham).

Enzyme-linked immunosorbent assay

Levels of IL-6, IL-1α and IL-1β of treated cells were determined by ELISA. The culture media of the treated cells were harvested and each cytokine was detected according to the manufacturer's protocol using Human Quantikine ELISA Kits (R&D Systems, Minneapolis, MN).

Adenoviral Vectors

Construction and characterization of adenoviral vectors encoding wild-type and dominant negative NADPH oxidase-4 (NOX4) have each been described previously (10, 21). An empty vector lacking the NOX4 construct was used as a control. All vectors were obtained from the University of Iowa Gene Vector Core. HNSCC cells in serum free media were infected with 100 MOI of the above described adenoviral vectors for 24 hours. Biochemical analyses were performed 72–96 h after transfection.

siRNA/shRNA transfection

MyD88, TLR2, TLR5 and control siRNA (Santa Cruz) were transfected into HNSCC cells at a concentration of 40–80 nM with equal volume Lipofectamine RNAiMAX (Invitrogen). Cells were incubated in Opti-MEM for 4 hours prior to addition of siRNA and 16 hours after addition of siRNA. For shRNA transfection, SQ20B cells were transfected with 1μg/mL of psiRNA-h7SKGFPzeo, psiRNA-shMyD88, or psiRNA-shIL1R (Invivogen) in the presence of Opti-MEM and Lipofectamine RNAiMAX. Cells were allowed to recover 48–72 hours in antibiotic-free DMEM with 10% FBS before 48-hour erlotinib treatment. Knockdown was confirmed by RT-PCR and/or western blot.

Clonogenic survival assay

Clonogenic survival was determined as previously described (22). Individual assays were performed with multiple dilutions with at least four cloning dishes per data point, repeated in at least 3 separate experiments.

Tumor cell implantation

Male and female athymic-*nu/nu* mice (4–5 weeks old) were purchased from Harlan Laboratories (Indianapolis, IN). Mice were housed in a pathogen-free barrier room in the Animal Care Facility at the University of Iowa and handled using aseptic procedures. All procedures were approved by the IACUC committee of the University of Iowa and conformed to the guidelines established by the NIH. Mice were allowed at least 3 days to acclimate prior to beginning experimentation, and food and water were made freely available. Tumor cells were inoculated into nude mice by subcutaneous injection of 0.1 mL aliquots of saline containing 2×10^6 SQ20B cells into the right flank using 26-gauge needles.

In vivo drugs administration

Mice started drug treatment 1 week after tumor inoculation. For the MyD88 knockdown experiments, female mice were randomized into 2 treatment groups and orally administered either water or 12.5 mg/kg erlotinib (ERL) daily. For the IL-1α neutralization experiments, male and female mice were randomized into 4 treatment groups as follows. Control group: Mice were administered water orally daily and 1 mg/kg IgG i.p once per week. Neutralizing IL-1α antibody (nIL-1αab) group: A human IL-1α neutralizing antibody (XBiotech; Austin, TX) was administered i.p. at 100 ug/mouse once per week. ERL group: ERL was administered orally 12.5 mg/kg daily. ERL+nIL-1αab group: ERL was administered orally 12.5 mg/kg daily in addition to nIL-1αab administered i.p. at 100 ug/mouse once per week. For experiments involving cetuximab (CTX), CTX was administered i.p. 2 mg per mouse twice per week and control mice were given IgG twice per week. All treatments were given for the duration of three weeks. Mice were evaluated daily and tumor measurements taken three times per week using Vernier calipers. Tumor volumes were calculated using the formula: tumor volume = (length × width^2)/2 where the length was the longest dimension, and width was the dimension perpendicular to length. Mice were euthanized via CO_2 gas asphyxiation or lethal overdose of sodium pentobarbital (100 mg/kg) when tumor diameter exceeded 1.5 cm in any dimension.

Bioinformatics

The Cancer Genome Browser (University of California-Santa Cruz; https://genome-cancer.ucsc.edu) was used to download the level 3 dataset HNSCC dataset (TCGA_HNSC_exp_HiSeqV2_PANCAN) from The Cancer Genome Atlas (TCGA). RNAseq data was normalized across all TCGA cohorts and reported as log2 values. Corresponding level 3 clinical data was available for most of the 467 samples. Selected tumors (n=41) also had RNAseq data for matched normal tissue. Matched tumor and normal samples were analyzed. Linear fold change was calculated to emphasize difference between groups. Kaplan-Meier survival curves were generated by comparing survival of the highest

quartile of expressing tumors (for indicated gene) against the lowest quartile. In some cases, Kaplan-Meier curves were generated using an aggregate of several genes. The genes aggregated are as follows: TLR (TLR1,TLR2, TLR4,TLR5,TLR6,TLR7,TLR8,TLR9,TLR10), IL-18R (IL18Ra,IL18Rb), IL-1R survival curve (IL1R1,IL1RAP), IL-1α, IL-1β and IL-1RA/IL-1RN). Tumors were ranked according to expression of each gene, and ranks were averaged to determine highest and lowest quartile of tumors expressing the given receptor family.

Statistical Analysis

Statistical analysis was done using GraphPad Prism version 5 for Windows (GraphPad Software, San Diego, CA). Differences between 3 or more means were determined by one-way ANOVA with Tukey post-tests. Linear mixed effects regression models were used to estimate and compare the group-specific change in tumor growth curves. Differences in survival curves were determined by Mantel-Cox test. All statistical analysis was performed at the $p<0.05$ level of significance.

Results

Erlotinib induces processes involved in inflammation

Of the top ten upregulated cellular process networks identified by ERL treatment, 6 processes were related to immune response or inflammation for both cell lines (Figure 1A,B). The top ten significant diseases that were identified from ERL treatment were predominantly systemic inflammatory disorders in both cell lines such as rheumatic diseases/disorders (rheumatic arthritis, rheumatic fever, rheumatic heart disease) (Figure 1C,D). Similarly, the majority of the top ten upregulated canonical pathways were immune response/inflammation related in both cell lines which included IL-6 and IL-1 signaling in SQ20B cells (Figure 2A) and TLR and IL-1 signaling in Cal-27 cells (Figure 2B).

The top network identified for SQ20B and Cal-27 was the NF-kB, MyD88, I-kB, IRAK1/2, NF-kB2 (p100) network (Figure 2C) and TRAF6, TAK1(MAP3K7), NF-kB, I-kB, IKK-gamma network (Figure 2D) respectively. The genes and processes in these networks were both related to MyD88-dependent TLR signaling and NFkB activity (Supplementary Tables 2,3). Altogether, the gene expression analyses suggested that ERL activates inflammatory processes and pathways which may be mediated by MyD88.

Loss of MyD88 increases tumor sensitivity to erlotinib

We have previously shown that ERL induces the secretion of IL-6 and other proinflammatory cytokines via NFkB activation in HNSCC cells (10) which supports the gene expression results (Figure 1,2). Transient knockdown of MyD88 significantly suppressed baseline and ERL-induced IL-6 production in both SQ20B (Figure 3A) and Cal-27 cells (Figure 3B). MyD88 stable knockout clones (shMyD88#2, shMyD88#9) also demonstrated significantly reduced IL-6 in the absence and presence of ERL compared to control (Figure 3C) supporting the role of MyD88-dependent signaling in ERL-induced IL-6 production. Both MyD88 knockout clones showed reduced tumor growth when treated with ERL compared to ERL-treated control xenografts (Figure 3D–G). Notably, xenografts

bearing the shMyD88 #9 clone showed reduced tumor growth in both treated and untreated groups (Figure 3D,G). Altogether these results suggest that MyD88-dependent signaling is involved in ERL-induced IL-6 secretion and suppresses the anti-tumor activity of ERL.

TLR5 signaling may be involved in erlotinib-induced IL-6 secretion

A general trend of increased TLR, IL-1R and IL-18R RNA expression was found in HNSCC human tumors (obtained from the Tissue Procurement Core (TPC) in the Department of Pathology) compared to matched normal tissue (Figure 4A,B). Notably, both tumors showed large increases in expression of TLR2 compared to normal matched tissue (Figure 4A,B). IL-6 secretion was significantly increased after treatment with agonists to TLR1/2, TLR2/6 and TLR3 in all 3 cell lines (Figure 4C), although TLR5 appeared to be active in only SQ20B cells (Figure 4C). ERL increased TLR8 expression in SQ20B cells and TLR10 in Cal-27 cells although the absolute levels of these TLRs were very low and most likely not of biological significance (Figure 4D). As the TLR1/2 and TLR2/6 dimers both depend on TLR2, the activity of these dimers were suppressed using siRNA targeted to TLR2 (Figure 4E,F). Knockdown of TLR2 expression did not decrease ERL-induced IL-6 (Figure 4E). However, knockdown of TLR5 expression partially but significantly suppressed ERL-induced IL-6 secretion in SQ20B cells (Figure 4G,H) which was not observed in Cal-27 cells (data not shown). TLR3, which is not a MyD88-dependent receptor also was not involved in ERL-induced IL-6 in both cell lines (Supplementary Figure 1). Altogether, these results suggest that of the TLRs, only TLR5 signaling may contribute to IL-6 secretion induced by ERL in select HNSCC cell lines.

IL-1 signaling is critical for erlotinib-induced IL-6 expression in HNSCC cells

In order to investigate the contribution of other MyD88-dependent signaling pathways, the IL-18R and IL-1R pathways were studied. Neutralization of IL-18R in SQ20B (Figure 4I) and Cal-27 (Figure 4J) failed to suppress ERL-induced IL-6. However, anakinra, a recombinant IL-1R antagonist (IL-1RA/IL-1RN) significantly reduced baseline and ERL-induced IL-6 in both SQ20B (Figure 5A) and Cal-27 (Figure 5B). Additionally, transient (Supplementary Figure 2) and stable knockdown of the IL-1R suppressed ERL-induced IL-6 (Figure 5C) suggesting that IL-1R signaling may be involved in ERL-induced IL-6. Sequenced HNSCC tumors and matched normal tissue (n=40) were analyzed from The Cancer Genome Atlas (TCGA) for mRNA levels of ligands of the IL-1 pathway. IL-1α and IL-1β were found to be increased in tumors by 4.8 fold and 2.5 fold respectively compared to normal samples while IL-1RA/IL-1RN was decreased by 2.5 fold (Figure 5D). IL-1α was also upregulated in both HNSCC tumors analyzed in Figure 4A,B while IL-1β was only upregulated in one of these tumors (Supplementary Figure 3). IL-1α but not IL-1β was detectable after ERL treatment and increased across all time points measured in both cell lines (Figure 5E). Exogenous IL-1α increased IL-6 secretion in the presence and absence of ERL (Figure 5F) and blockade of IL-1α abut not of IL-1β activity significantly reduced IL-6 secretion in the absence and presence of ERL (Figure 5G) suggesting that IL-1α release may be responsible for ERL-induced IL-6 production.

Erlotinib-induced cell death triggers IL-1α release

IL-1α unlike IL-1β is not secreted but is typically released by cell death. To confirm this, we showed that Z-VAD-fmk (ZVAD), a pan-caspase inhibitor, significantly reduced baseline and ERL-induced levels of IL-1α (Figure 6A) and blocked ERL-induced cell death (Supplementary Figure 4) suggesting that IL-1α is likely released due to ERL-induced cell death. These results were not observed with the caspase-1 inhibitor, Ac-Y-VAD-cho (YVAD, Figure 6A). Our laboratory has previously shown that ERL induces cell death via hydrogen peroxide (H_2O_2)-mediated oxidative stress due to NADPH oxidase-4 (NOX4) activity (23). To confirm that oxidative stress is involved in IL-1α release we showed that the antioxidants NAC and CAT significantly suppressed ERL-induced IL-1α in addition to IL-6 in both SQ20B (Figure 6B) and Cal-27 cells (Figure 6C). We have previously shown that these antioxidants significantly protect these HNSCC cell lines from ERL-induced cytotoxicity (23). Moreover, overexpression of dominant negative NOX4 (N4dn) decreased ERL-induced IL-1α, IL-6 production (Figure 6D,E) and cytotoxicity (Figure 6F) in both SQ20B (Figure 6D,F) and Cal-27 (Figure 6E,F). The opposite results were observed with wildtype NOX4 (N4wt) (Figure 6D–F). The ability of N4wt (and not N4dn) to significantly induce oxidative stress in these cell lines has been demonstrated in our previous publications (10, 21). Altogether, these results suggest that ERL-induced oxidative stress (via NOX4) results in cell death leading to IL-1α release resulting in activation of IL-1R signaling in unaffected/surviving cells leading to IL-6 expression and secretion.

IL-1α is negatively correlated with survival in HNSCC

Sequenced HNSCC tumors (TCGA, n=467) with high expression of MyD88, TLRs, IL-1R, IL-18R, IL-1α, IL-1β and IL-1RA were plotted for survival against low expressing tumors (Figure 7A–H). MyD88, TLRs, IL-18R, IL-1β and IL-1RA were not significantly correlated with survival (Figure 7A–C, G,H). High IL-1R expressing tumors showed a trend (p=0.06) toward a negative correlation with survival (Figure 7D) while IL-1α mRNA expression was negatively correlated (p=0.04) with survival (Figure 7E). Selected tumors from patients that received targeted molecular therapy (TMT, n=40), showed an increased negative correlation with survival (p=0.02, Figure 7F) suggesting that IL-1α expression may be an important prognostic marker in HNSCC.

Finally, we showed that SQ20B cells treated with an IL-1α neutralizing antibody (XBiotech, Austin, TX (24)) in combination with ERL displayed a significant reduction in survival compared to the other treatment groups *in vitro* (Figure 7I) and *in vivo* (Figure 7J). Similar results were observed with CTX *in vivo* (Figure 7K) suggesting that blockade of the IL-1 pathway may increase the sensitivity of ERL and other EGFRIs. Altogether, our results and previous findings suggest that ERL (and perhaps other EGFRIs) induce cell death via H_2O_2-mediated oxidative stress due to NOX4 activity leading to IL-1α release and activation of the IL-1R/MyD88/NFkB signaling axis on surviving tumor cells resulting in IL-6 secretion (Figure 7L). Our results also propose that another unidentified DAMP may be released that activates the TLR5/MyD88/NFkB signaling axis resulting in IL-6 secretion. This IL-6 signaling is believed to reduce the anti-tumor activity of EGFRIs and promote tumor progression (Figure 7L).

Discussion

Our lab has previously shown that EGFRIs increased IL-6 secretion and that IL-6 levels played a critical role in the anti-tumor effect of ERL *in vitro* and *in vivo* (10) which has been supported and studied in depth by other groups (15–18). The studies presented here now indicate that MyD88-dependent IL-1R signaling is most likely responsible for the IL-6 production induced by EGFRIs. Therefore targeting IL-1 signaling may be a novel strategy to increase the anti-tumor efficacy of ERL and other EGFRIs in HNSCC.

We have observed that the majority of cellular processes and pathways upregulated by ERL treatment were related to immune response and inflammation (Figure 1,2). These observations support one other study showing that the EGFRI PD153035 upregulated genes related to inflammation and innate immunity (25). Interestingly, the inflammatory profile displayed by ERL treatment was remarkably similar to that of rheumatic diseases and other systemic inflammatory disorders (Figure 1C,D). In fact, inhibition of the IL-1 pathway is a well-documented strategy for the treatment of rheumatoid arthritis (RA) since IL-1R ligands (IL-1α and IL-1β) are particularly abundant in the synovial lining of the joint (26). Anakinra is a humanized recombinant IL-1R antagonist (IL-1RA) that is FDA approved for use in the treatment of RA. IL-1RA is an IL-1R ligand that inhibits the IL-1 pathway through competition with the other IL-1R ligands (27). In support of this, we have shown that anakinra effectively blocked ERL-induced IL-6 in HNSCC cell lines (Figure 5A,B) implying that IL-1 pathway-targeting drugs used for the management of RA (and other systemic inflammatory disorders) could be investigated as a potential adjuvant to EGFRIs in the treatment of HNSCC.

Of the ligands in the IL-1 family, IL-1β is the most well-studied and its production is dependent on inflammasome-mediated caspase-1 activity (28). In the present studies we believe that IL-1α and not IL-1β is involved in the activation of the IL-1R/MyD88/IL-6 pathway by ERL since we were unable to detect any secreted IL-1β and suppression of IL-1β using a neutralizing IL-1β antibody or a caspase-1 inhibitor did not affect ERL-induced IL-6 (Figure 4E,G; Figure 6A). On the other hand, we were able to detect IL-1α (Figure 5E) and suppression of IL-1α significantly blocked ERL-induced IL-6 (Figure 5G) suggesting that IL-1α was the ligand responsible for activating the IL-1 pathway.

Unlike IL-1β, IL-1α is not secreted from the cell, but is released during cell death and acts as a DAMP (29). It is likely that the cell death induced by ERL treatment resulted in IL-1α release since the use of ZVAD blocked ERL-induced cell death (Supplementary Figure 4) and IL-1α release (Figure 6A). Furthermore, our laboratory has previously shown that ERL induces cell death via H_2O_2-mediated oxidative stress due to NOX4 activity (23). We have now extended these findings to show that IL-1α release in addition to downstream IL-6 secretion is mediated by ERL-induced cell death due to NOX4-induced oxidative stress (Figure 6B–F).

Our gene expression analyses also implicated TLR/MyD88 signaling (especially TLR2) as a possible mediator ERL-induced IL-6 (Figure 2) however we found no evidence of TLR2 involvement despite TLR2 being present and active on HNSCC tumors and cell lines

(Figure 4A–C). Surprisingly, we found that TLR2 knockdown increased IL-6 secretion (Figure 4E). An explanation for these results is unclear although one prior report has shown that activation of TLR2 resulted in decreased NFkB activity via increased miR-329 leading to decreased IL-6 expression in human trophoblast cells (30). Perhaps in our HNSCC cell model, inhibition of TLR2 expression decreased levels of miR-329 resulting in increased NFkB and IL-6 secretion, which would be consistent with the previous findings in trophoblast cells (30). Interestingly, TLR5 was active in only SQ20B cells (Figure 4C) and TLR5 knockdown partially but significantly suppressed ERL-induced IL-6 production in this cell line only suggesting that TLR5 activity may be important in select HNSCC cell lines (Figure 4G,H). At this time, endogenous DAMPS capable of activation of TLR5 are unknown, therefore we are unclear as to how ERL induces TLR5.

Given that IL-1α appears to be the ligand that triggers the IL-1R/MyD88/IL-6 cascade that we believe is responsible for poor response to EGFRIs, then in theory, neutralization of IL-1α should increase the anti-tumor efficacy of EGFRIs in the same manner as blockade of IL-6 as previously shown by our laboratory (10, 15–18). Indeed we observed that IL-1α neutralization significantly increased the anti-tumor efficacy of ERL (Figure 7J) in addition to CTX (Figure 7K) in SQ20B cells. These exciting results suggest that IL-1α plays an important role in response to EGFRIs. Moreover, we want to highlight that the observed effects of ERL in our studies are believed to be directly due to cell death mediated by EGFR inhibition and not due to off-target effects of the drugs since 1: we are using clinical achievable doses (31) and 2: we have already confirmed the ability of EGFR knockdown (using siRNA targeted to EGFR) to induce oxidative stress, cell death and cytokine secretion (10, 23).

To further stress the importance of IL-1α in the management of HNSCC, we found that HNSCC tumors expressed high levels of IL-1α compared to matched normal tissue (Figure 5D) and high-IL-1α-expressing tumors have worse prognosis than low-IL-1α-expressing tumors (Figures 7E). Furthermore, when we selected for tumors from patients receiving TMT, we found an increased separation and significance between the survival curves (Figure 7F) suggesting that IL-1α expression may not only predict overall survival in HNSCC but also predict response to TMT. Unfortunately, the clinical information associated with the tumors from patients that received TMT did not reveal what treatment regimen was administered therefore we cannot make firm conclusions from this analysis. However since the only TMT currently used in HNSCC is EGFR-targeting drugs and the only approved EGFRI for HNSCC to date is CTX, it is more likely than not that the TMT involved CTX in our analysis.

Suppression of MyD88 effectively blocked ERL-induced IL-6 production and suppressed tumor growth in the presence of ERL (Figure 3), which is likely due to the ability of MyD88 knockdown to block all potential pro-inflammatory signaling from MyD88-dependent receptors. It is unclear why control-treated shMyD88 #9 tumors displayed such a pronounced inhibition of tumor growth (Figure 3E) compared to control-treated shMyD88 #2 tumors (Figure 3D). Previous reports have shown that MyD88 signaling may induce EGFR ligands such as amphiregulin (AREG) and epiregulin (EREG) resulting in the activation of EGFR (32). Perhaps knockdown of MyD88 expression in the shMyD88 #9

clone led to the inhibition of EGFR via downregulation of AREG/EREG in addition to suppression of IL-6, which may explain our observations. Nevertheless, these results suggest that MyD88 inhibition may also be a promising strategy to increase the effect of ERL.

It should be noted that global inhibition of MyD88, IL-1α or any factor in the IL-1R/MyD88/IL-6 signaling axis *in vivo* may have unexpected results. Our model takes into account only the activity of MyD88 or IL-1α within cancer cells. Inhibition of these inflammatory components in innate immune cells may change the inflammatory microenvironment especially in an immune competent mouse model, conceivably altering recruitment of immune cells and unpredictably altering growth of the tumor. This remains to be studied.

Based on these findings and our prior studies (10, 21, 23), we propose a model in which EGFR inhibition causes cell death and release of IL-1α which we believe binds its receptor IL-1R on surviving cells, activates MyD88 and induces IL-6 secretion via NFkB (Figure 7L). IL-6 signaling pathways typically lead to phosphorylation of STAT3, which is well known to compensating for the loss of EGFR signaling due to cross talk (33). As such, we believe that the poor response and possibly acquired resistance to ERL in the clinical setting may be due to IL-1R/MyD88/IL-6 signaling triggered by release of IL-1α from dying cells, which is different from other proposed mechanisms of poor response/acquired resistance (acquired mutations, alternative signaling pathways (6–9)). To our knowledge, the studies presented here are the first to connect IL-1α and MyD88-dependent signaling with response to EGFR-targeted therapy and this novel mechanism may offer insight into why other methods of overcoming EGFRI resistance have failed, and proposes new clinical targets that may enhance the efficacy of EGFRIs in HNSCC.

Supplementary Material

Refer to Web version on PubMed Central for supplementary material.

Acknowledgments

The authors thank Dr. Thomas Bair in the Bioinformatics Division at The University of Iowa for his assistance in analyzing the microarray studies and Dr. C. Michael Knudson, Rita Sigmund and Joe Galbraith from the Tumor Procurement Core (TPC) in the Department of Pathology for providing the HNSCC tumor samples. The authors also thank Dr. Sushma Shivaswamy and Mr. John Simard for kindly providing the human neutralizing IL-1α antibody for use in our *in vivo* studies. Finally, we thank Nicholas Borcherding and Drs. Weizhou Zhang, Fayyaz Sutterwala and Hasem Habelhah for their helpful suggestions and discussions regarding this work.

Grant Support

This work was supported by grants NIH R01DE024550, NIH K01CA134941 and IRG-77-004-34 from the American Cancer Society, administered through the Holden Comprehensive Cancer Center at the University of Iowa.

References

1. Loeffler-Ragg J, Schwentner I, Sprinzl GM, Zwierzina H. EGFR inhibition as a therapy for head and neck squamous cell carcinoma. Expert Opin Investig Drugs. 2008; 17:1517–31.

2. Bonner JA, Harari PM, Giralt J, Azarnia N, Shin DM, Cohen RB, et al. Radiotherapy plus cetuximab for squamous-cell carcinoma of the head and neck. N Engl J Med. 2006; 354:567–78. [PubMed: 16467544]

3. Cohen EE, Kane MA, List MA, Brockstein BE, Mehrotra B, Huo D, et al. Phase II trial of gefitinib 250 mg daily in patients with recurrent and/or metastatic squamous cell carcinoma of the head and neck. Clin Cancer Res. 2005; 11:8418–24. [PubMed: 16322304]

4. Soulieres D, Senzer NN, Vokes EE, Hidalgo M, Agarwala SS, Siu LL. Multicenter phase II study of erlotinib, an oral epidermal growth factor receptor tyrosine kinase inhibitor, in patients with recurrent or metastatic squamous cell cancer of the head and neck. J Clin Oncol. 2004; 22:77–85. [PubMed: 14701768]

5. Vermorken JB, Trigo J, Hitt R, Koralewski P, Diaz-Rubio E, Rolland F, et al. Open-label, uncontrolled, multicenter phase II study to evaluate the efficacy and toxicity of cetuximab as a single agent in patients with recurrent and/or metastatic squamous cell carcinoma of the head and neck who failed to respond to platinum-based therapy. J Clin Oncol. 2007; 25:2171–7. [PubMed: 17538161]

6. Argiris A, Kotsakis AP, Hoang T, Worden FP, Savvides P, Gibson MK, et al. Cetuximab and bevacizumab: preclinical data and phase II trial in recurrent or metastatic squamous cell carcinoma of the head and neck. Ann Oncol. 2013; 24:220–5. [PubMed: 22898037]

7. de Souza JA, Davis DW, Zhang Y, Khattri A, Seiwert TY, Aktolga S, et al. A phase II study of lapatinib in recurrent/metastatic squamous cell carcinoma of the head and neck. Clin Cancer Res. 2012; 18:2336–43. [PubMed: 22371453]

8. Miller VA, Hirsh V, Cadranel J, Chen YM, Park K, Kim SW, et al. Afatinib versus placebo for patients with advanced, metastatic non-small-cell lung cancer after failure of erlotinib, gefitinib, or both, and one or two lines of chemotherapy (LUX-Lung 1): a phase 2b/3 randomised trial. Lancet Oncol. 2012; 13:528–38. [PubMed: 22452896]

9. Ross HJ, Blumenschein GR Jr, Aisner J, Damjanov N, Dowlati A, Garst J, et al. Randomized phase II multicenter trial of two schedules of lapatinib as first- or second-line monotherapy in patients with advanced or metastatic non-small cell lung cancer. Clin Cancer Res. 2010; 16:1938–49. [PubMed: 20215545]

10. Fletcher EV, Love-Homan L, Sobhakumari A, Feddersen CR, Koch AT, Goel A, et al. EGFR inhibition induces proinflammatory cytokines via NOX4 in HNSCC. Mol Cancer Res. 2013; 11:1574–84. [PubMed: 24048704]

11. Duffy SA, Taylor JM, Terrell JE, Islam M, Li Y, Fowler KE, et al. Interleukin-6 predicts recurrence and survival among head and neck cancer patients. Cancer. 2008; 113:750–7. [PubMed: 18536030]

12. Heimdal JH, Kross K, Klementsen B, Olofsson J, Aarstad HJ. Stimulated monocyte IL-6 secretion predicts survival of patients with head and neck squamous cell carcinoma. BMC Cancer. 2008; 8:34. [PubMed: 18234094]

13. Kamimura D, Ishihara K, Hirano T. IL-6 signal transduction and its physiological roles: the signal orchestration model. Rev Physiol Biochem Pharmacol. 2003; 149:1–38. [PubMed: 12687404]

14. Riedel F, Zaiss I, Herzog D, Gotte K, Naim R, Hormann K. Serum levels of interleukin-6 in patients with primary head and neck squamous cell carcinoma. Anticancer Res. 2005; 25:2761–5. [PubMed: 16080523]

15. Giles KM, Kalinowski FC, Candy PA, Epis MR, Zhang PM, Redfern AD, et al. Axl mediates acquired resistance of head and neck cancer cells to the epidermal growth factor receptor inhibitor erlotinib. Mol Cancer Ther. 2013; 12:2541–58. [PubMed: 24026012]

16. Lee HJ, Zhuang G, Cao Y, Du P, Kim HJ, Settleman J. Drug resistance via feedback activation of Stat3 in oncogene-addicted cancer cells. Cancer Cell. 2014; 26:207–21. [PubMed: 25065853]

17. Li L, Han R, Xiao H, Lin C, Wang Y, Liu H, et al. Metformin sensitizes EGFR-TKI-resistant human lung cancer cells in vitro and in vivo through inhibition of IL-6 signaling and EMT reversal. Clin Cancer Res. 2014; 20:2714–26. [PubMed: 24644001]

18. Yao Z, Fenoglio S, Gao DC, Camiolo M, Stiles B, Lindsted T, et al. TGF-beta IL-6 axis mediates selective and adaptive mechanisms of resistance to molecular targeted therapy in lung cancer. Proc Natl Acad Sci U S A. 2010; 107:15535–40. [PubMed: 20713723]

19. Martin MU, Wesche H. Summary and comparison of the signaling mechanisms of the Toll/interleukin-1 receptor family. Biochim Biophys Acta. 2002; 1592:265–80. [PubMed: 12421671]
20. Weichselbaum RR, Dahlberg W, Beckett M, Karrison T, Miller D, Clark J, et al. Radiation-resistant and repair-proficient human tumor cells may be associated with radiotherapy failure in head- and neck-cancer patients. Proc Natl Acad Sci U S A. 1986; 83:2684–8. [PubMed: 3458227]
21. Sobhakumari A, Schickling BM, Love-Homan L, Raeburn A, Fletcher EV, Case AJ, et al. NOX4 mediates cytoprotective autophagy induced by the EGFR inhibitor erlotinib in head and neck cancer cells. Toxicol Appl Pharmacol. 2013; 272:736–45. [PubMed: 23917044]
22. Spitz DR, Malcolm RR, Roberts RJ. Cytotoxicity and metabolism of 4-hydroxy-2-nonenal and 2-nonenal in H2O2-resistant cell lines. Do aldehydic by-products of lipid peroxidation contribute to oxidative stress? Biochem J. 1990; 267:453–9. [PubMed: 2334404]
23. Orcutt KP, Parsons AD, Sibenaller ZA, Scarbrough PM, Zhu Y, Sobhakumari A, et al. Erlotinib-mediated inhibition of EGFR signaling induces metabolic oxidative stress through NOX4. Cancer Res. 2011; 71:3932–40. [PubMed: 21482679]
24. Hong DS, Hui D, Bruera E, Janku F, Naing A, Falchook GS, et al. MABp1, a first-in-class true human antibody targeting interleukin-1alpha in refractory cancers: an open-label, phase 1 dose-escalation and expansion study. The Lancet Oncology. 2014; 15:656–66. [PubMed: 24746841]
25. Woodworth CD, Michael E, Marker D, Allen S, Smith L, Nees M. Inhibition of the epidermal growth factor receptor increases expression of genes that stimulate inflammation, apoptosis, and cell attachment. Mol Cancer Ther. 2005; 4:650–8. [PubMed: 15827339]
26. Burmester GR, Feist E, Dorner T. Emerging cell and cytokine targets in rheumatoid arthritis. Nat Rev Rheumatol. 2014; 10:77–88. [PubMed: 24217582]
27. Boraschi D, Tagliabue A. The interleukin-1 receptor family. Semin Immunol. 2013; 25:394–407. [PubMed: 24246227]
28. Bergsbaken T, Fink SL, Cookson BT. Pyroptosis: host cell death and inflammation. Nat Rev Microbiol. 2009; 7:99–109. [PubMed: 19148178]
29. Kim B, Lee Y, Kim E, Kwak A, Ryoo S, Bae SH, et al. The Interleukin-1alpha Precursor is Biologically Active and is Likely a Key Alarmin in the IL-1 Family of Cytokines. Front Immunol. 2013; 4:391. [PubMed: 24312098]
30. Garg M, Potter JA, Abrahams VM. Identification of microRNAs that regulate TLR2-mediated trophoblast apoptosis and inhibition of IL-6 mRNA. PLoS One. 2013; 8:e77249. [PubMed: 24143215]
31. Hidalgo M, Siu LL, Nemunaitis J, Rizzo J, Hammond LA, Takimoto C, et al. Phase I and pharmacologic study of OSI-774, an epidermal growth factor receptor tyrosine kinase inhibitor, in patients with advanced solid malignancies. J Clin Oncol. 2001; 19:3267–79. [PubMed: 11432895]
32. Brandl K, Sun L, Neppl C, Siggs OM, Le Gall SM, Tomisato W, et al. MyD88 signaling in nonhematopoietic cells protects mice against induced colitis by regulating specific EGF receptor ligands. Proc Natl Acad Sci U S A. 2010; 107:19967–72. [PubMed: 21041656]
33. Colomiere M, Ward AC, Riley C, Trenerry MK, Cameron-Smith D, Findlay J, et al. Cross talk of signals between EGFR and IL-6R through JAK2/STAT3 mediate epithelial-mesenchymal transition in ovarian carcinomas. Br J Cancer. 2009; 100:134–44. [PubMed: 19088723]

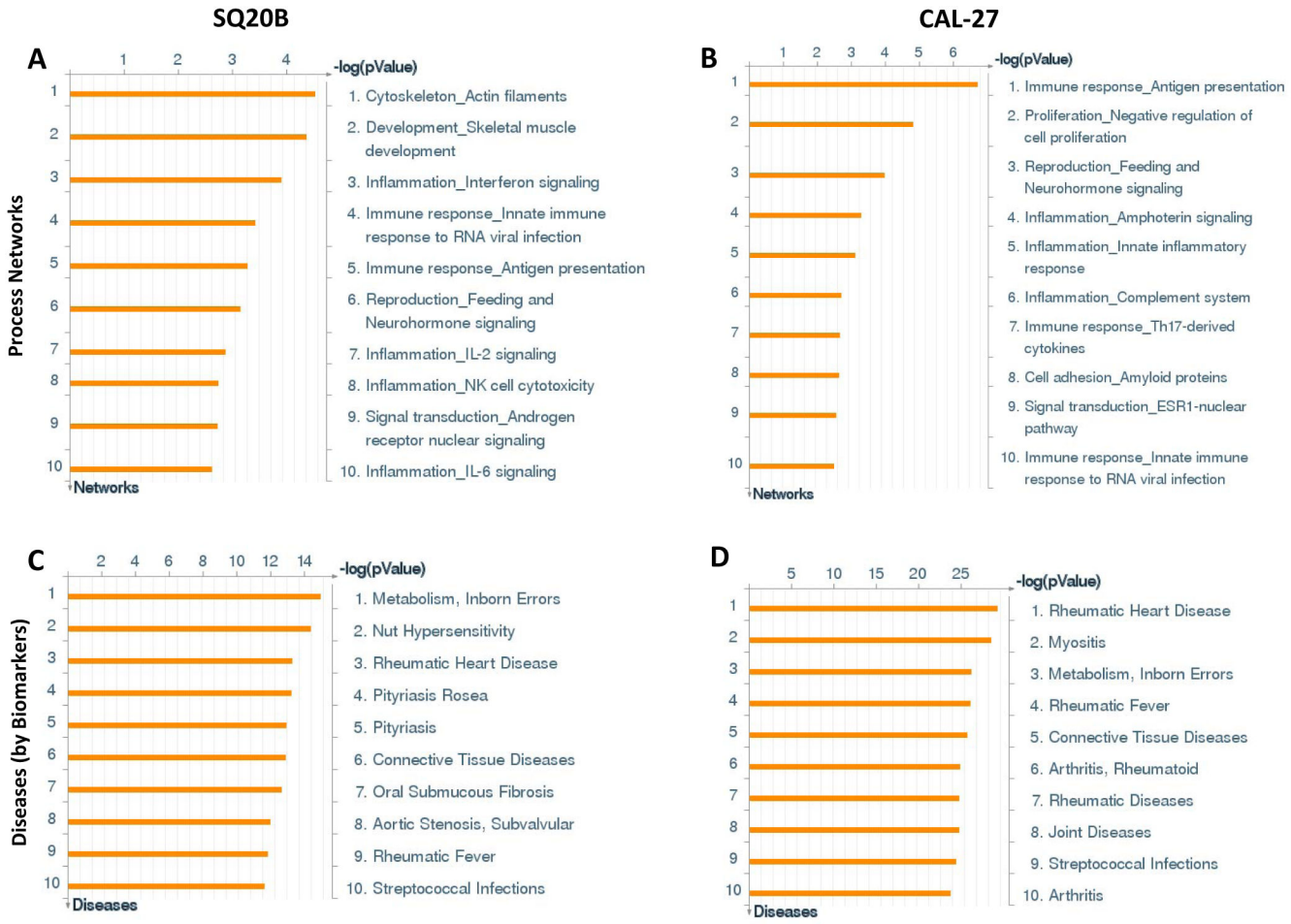

Figure 1. Process network and disease analyses of erlotinib-treated HNSCC cells

Shown are the top ten upregulated cellular/molecular processes (A,B) and diseases (C,D) from differentially regulated transcripts comparing microarray data from erlotinib (5 μM, 48 h) treated SQ20B (A,C) and Cal-27 (B,D) head and neck squamous carcinoma cells versus DMSO treated cells.

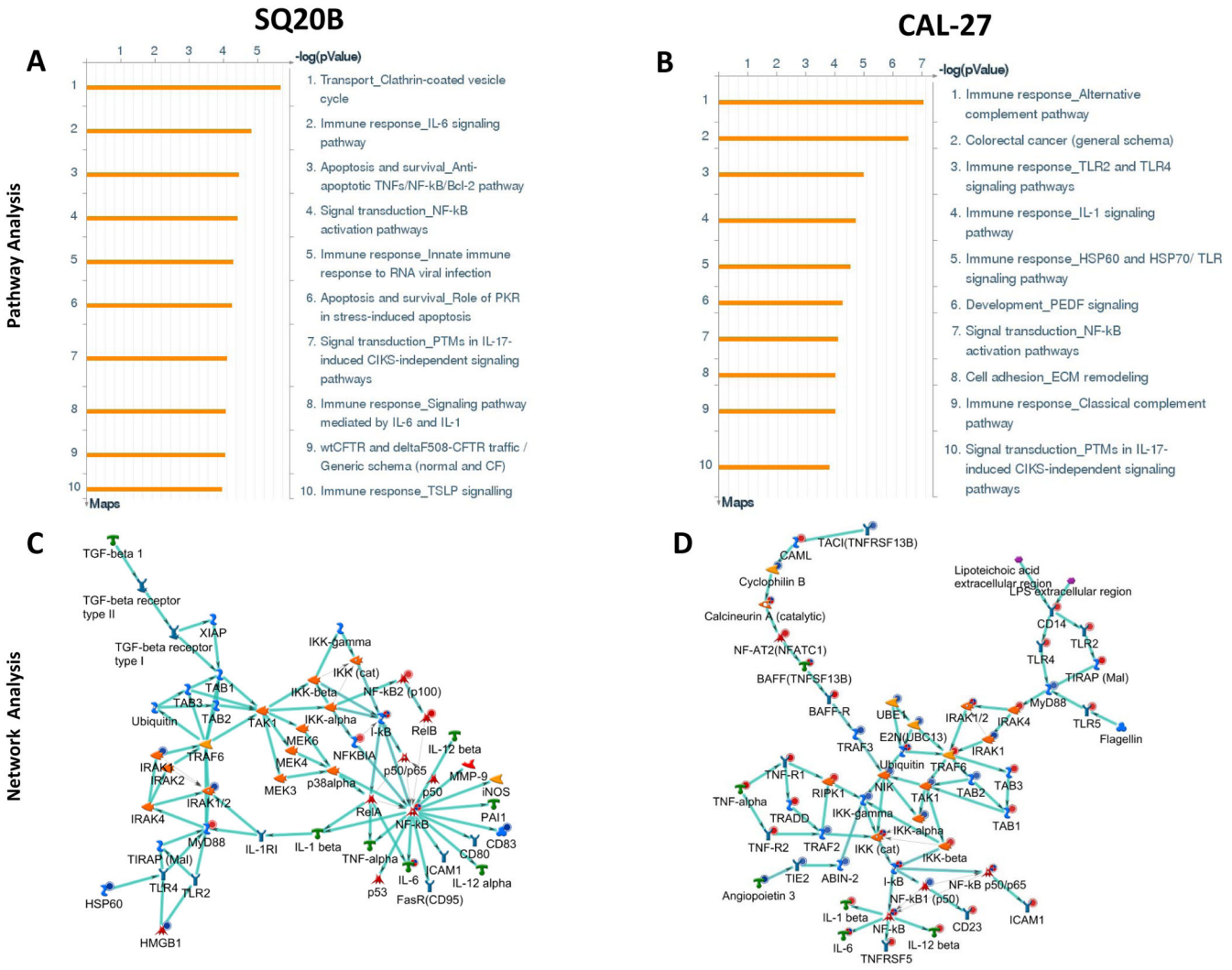

Figure 2. Pathway and network analysis of erlotinib-treated HNSCC cells

Shown are the top ten upregulated pathways (A,B) and top upregulated inflammation-related networks (C,D) constructed from differentially regulated transcripts comparing microarray data from erlotinib (5 μM, 48 h) treated SQ20B (A,C) and Cal-27 (B,D) head and neck squamous carcinoma cells versus DMSO treated cells. Up regulated genes are marked with red circles; down regulated with blue circles. The ‘checkerboard’ color indicates mixed expression for the gene between cell lines.

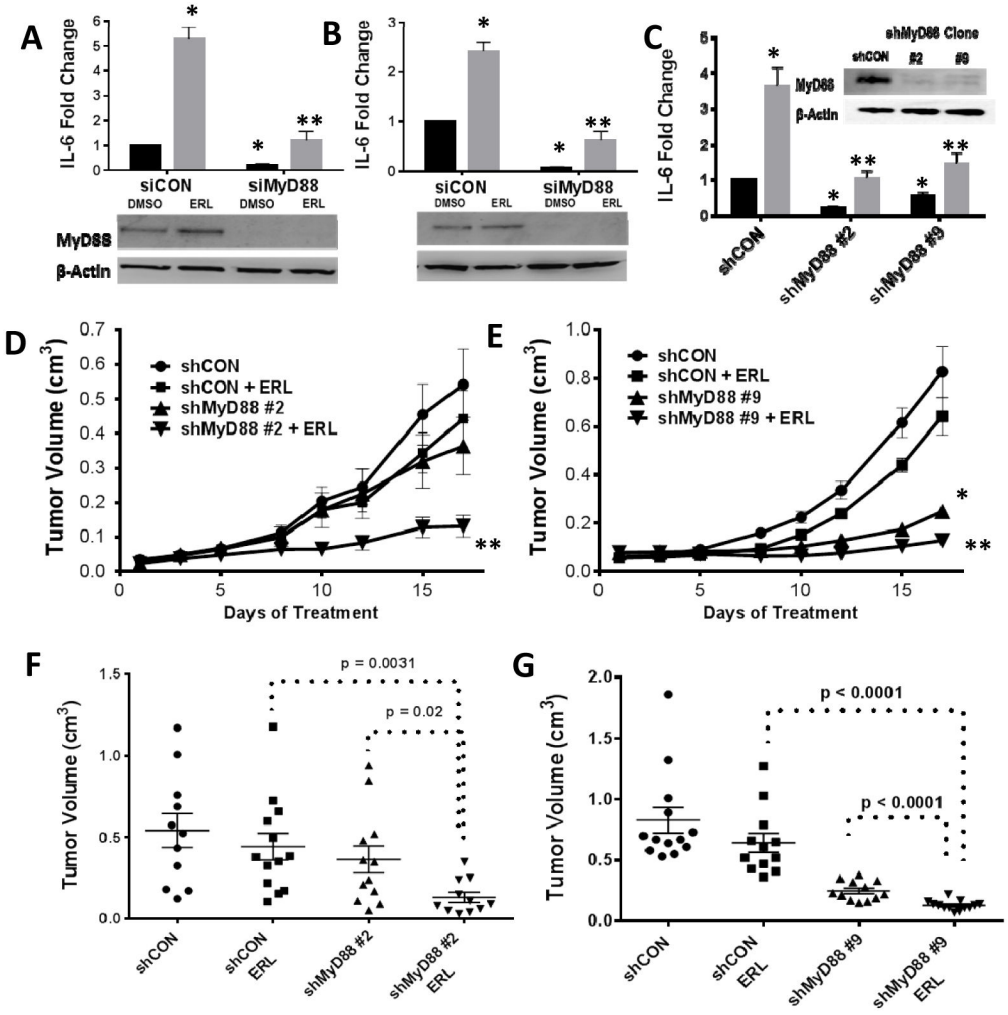

Figure 3. Knockdown of MyD88 reduces IL-6 and tumor growth in HNSCC cells

SQ20B (A) and Cal-27 (B) cells were transfected with scrambled siRNA control (siCON), or siRNA targeted against MyD88 (siMyD88). Cells were treated with DMSO (black bars) or erlotinib ([ERL], 5μM; gray bars) for 48 hours and IL-6 measured by ELISA. SQ20B cells were transfected with a shRNA targeted against MyD88 (shMyD88), or a control plasmid (shCON), and selected with zeocin. Clones were analyzed for MyD88 levels by Western blot (C inset) and IL-6 in the presence of DMSO and 5 μM ERL (C). D–G: The above clones were injected into the right flank of athymic *nu/nu* mice. Tumor growth was measured over a three week treatment period (12.5 mg/kg ERL or water daily) (D,E). Tumor volume at Day 17 is shown for clone #2 (F) and clone #9 (G). N = 11–13. Error bars = standard error of the mean (SEM). *p<0.05 versus control; **p<0.05 versus ERL.

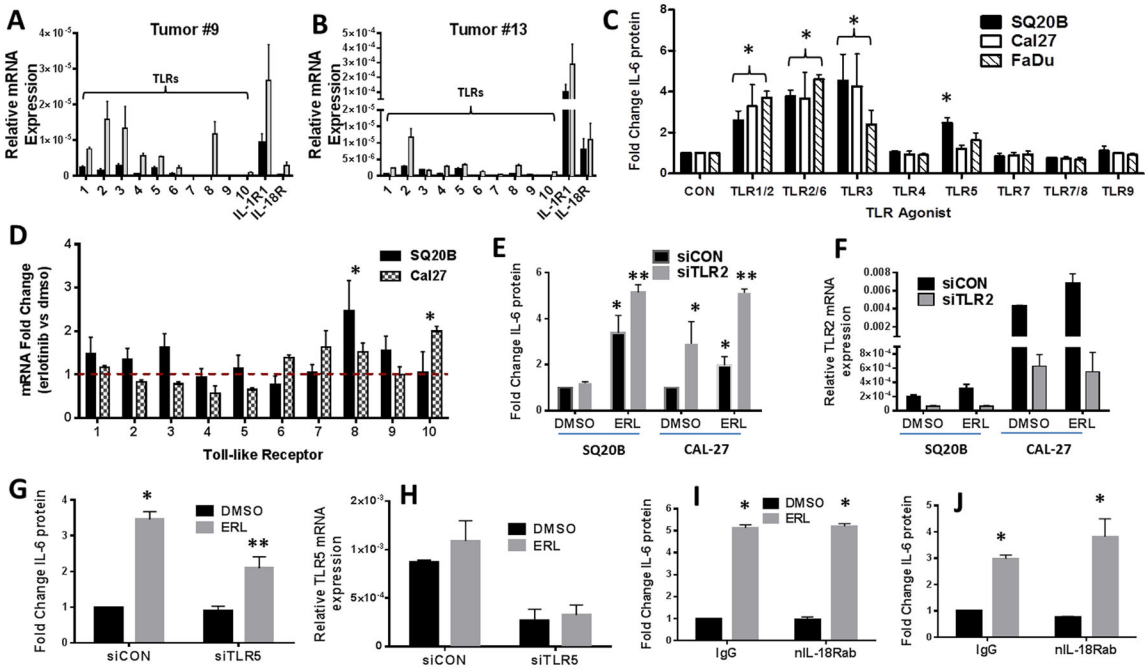

Figure 4. Role of TLR signaling in erlotinib-induced IL-6 in HNSCC cells

A,B: RNA isolated from two HNSCC tumors (#9 (A) and #13 (B)) (gray bars) and matched normal tissue (black bars) was analyzed for TLR1-10, IL-1R and IL-18R gene expression by RTPCR. C: SQ20B, Cal27 and FaDu cells were treated with TLR agonists as described in the Methods section. Secreted IL-6 was measured by ELISA. D: SQ20B and Cal-27 were treated with DMSO or 5μM erlotinib (ERL) for 48 hours. Cells were analyzed by RTPCR for expression of TLR genes. Values were normalized to 18S mRNA levels, and reported as fold change over DMSO (set at 1, dotted line). E–H: SQ20B or Cal-27 cells were transfected with scrambled siRNA control (siCON), siRNA targeted against TLR2 (siTLR2) (E,F), or siRNA targeted against TLR5 (siTLR5) (G,H), treated with DMSO or 5μM ERL, then analyzed for IL-6. Knockdown of respective TLRs were confirmed by RTPCR (F,H). SQ20B (I) and Cal27 (J) cells were treated with IgG or an IL-18R neutralizing antibody (nIL-18Rab, 0.5 ug/mL) for two hours prior to DMSO or ERL (5μM) before IL-6 analysis. N=3, errors bars = standard error of the mean (SEM). *p<0.05 versus control; **p<0.05 versus ERL.

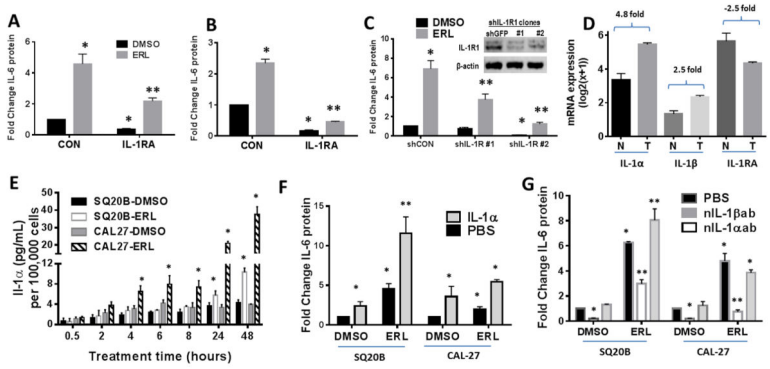

Figure 5. Role of IL-1 signaling in erlotinib-induced IL-6 secretion

SQ20B (A) and Cal27 (B) cells were treated with DMSO (CON) or 50 ng/mL and 10 ng/mL respectively of anakinra (IL-1RA) for two hours followed by 48 hour treatment with DMSO or erlotinib ([ERL], 5 μM) then analysis for IL-6 secretion by ELISA. C: SQ20B cells were transfected with shRNA targeted against IL-1R1 (shIL-1R1), or a control plasmid (shCON/shGFP), and selected with zeocin. Clones were analyzed for IL-1R1 levels by western blot (C inset) and IL-6 levels. A dataset (n=41) of HNSCC tumors (T) and matched normal tissue (N) from The Cancer Genome Atlas was analyzed for expression of IL-1α, IL-1β, and IL-1RA mRNA. Linear fold change (tumor over normal) is reported (D). E: Cell lines were treated with DMSO or 5 μM ERL for the indicated time points and analyzed for IL-1α by ELISA. F: Cells were treated with PBS or 1 ng/mL human recombinant IL-1α for two hours, treated with DMSO or ERL, then analyzed for IL-6 secretion. G: Cells were treated with anti-IL-1α or anti-IL-1β neutralizing antibodies for two hours prior to treatment with DMSO or ERL then analyzed for IL-6. N=3, errors bars = SEM. *p<0.05 versus control; **p<0.05 versus ERL.

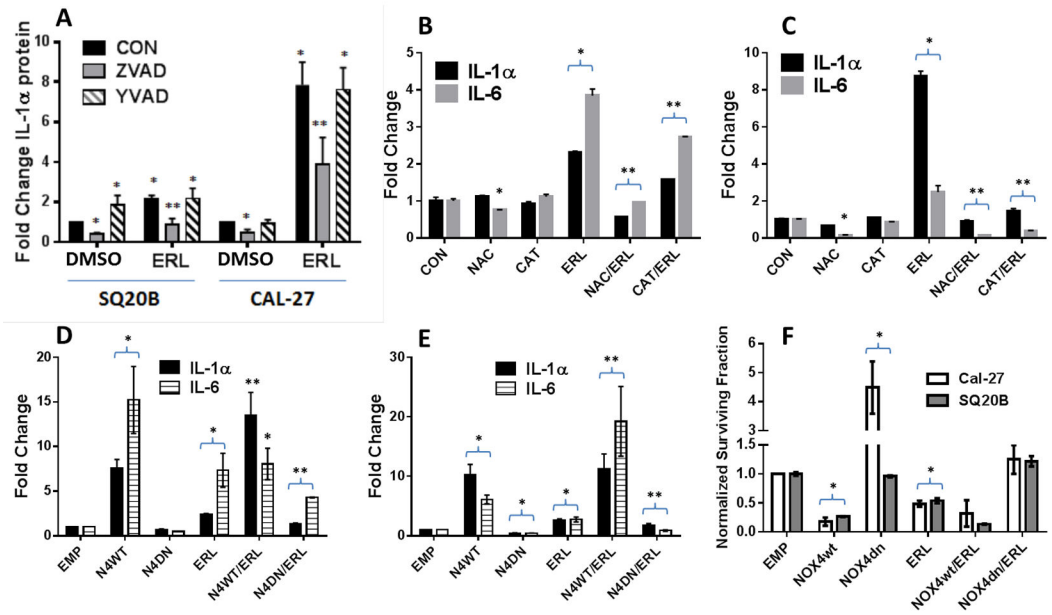

Figure 6. Erlotinib increases IL-1α secretion via oxidative stress-mediated cell death

A: SQ20B and Cal-27 cells were pre-treated with Z-VAD-fmk (ZVAD) or Y- VAD-fmk (YVAD) for one hour prior to 48-hour DMSO or 5 μM erlotinib (ERL) then analyzed for IL-1α by ELISA. B,C: SQ20B (B) and Cal-27 (C) cells were pre-treated with 20 mM N-acetyl cysteine (NAC) or 100 U/mL pegylated catalase (CAT) for 1 h before treatment with ERL, then analyzed for IL-1α and IL-6 secretion by ELISA. D-F: SQ20B (D) and Cal-27 (E) were transfected with empty (EMP), wildtype NADPH oxidase-4 (N4wt) or dominant negative NOX4 (N4dn) adenoviral vectors before treatment with DMSO or ERL, then analysis for IL-1α and IL-6 secretion by ELISA (D,E) and clonogenic survival (F). N=3, errors bars = SEM. *p<0.05 versus control; **p<0.05 versus ERL.

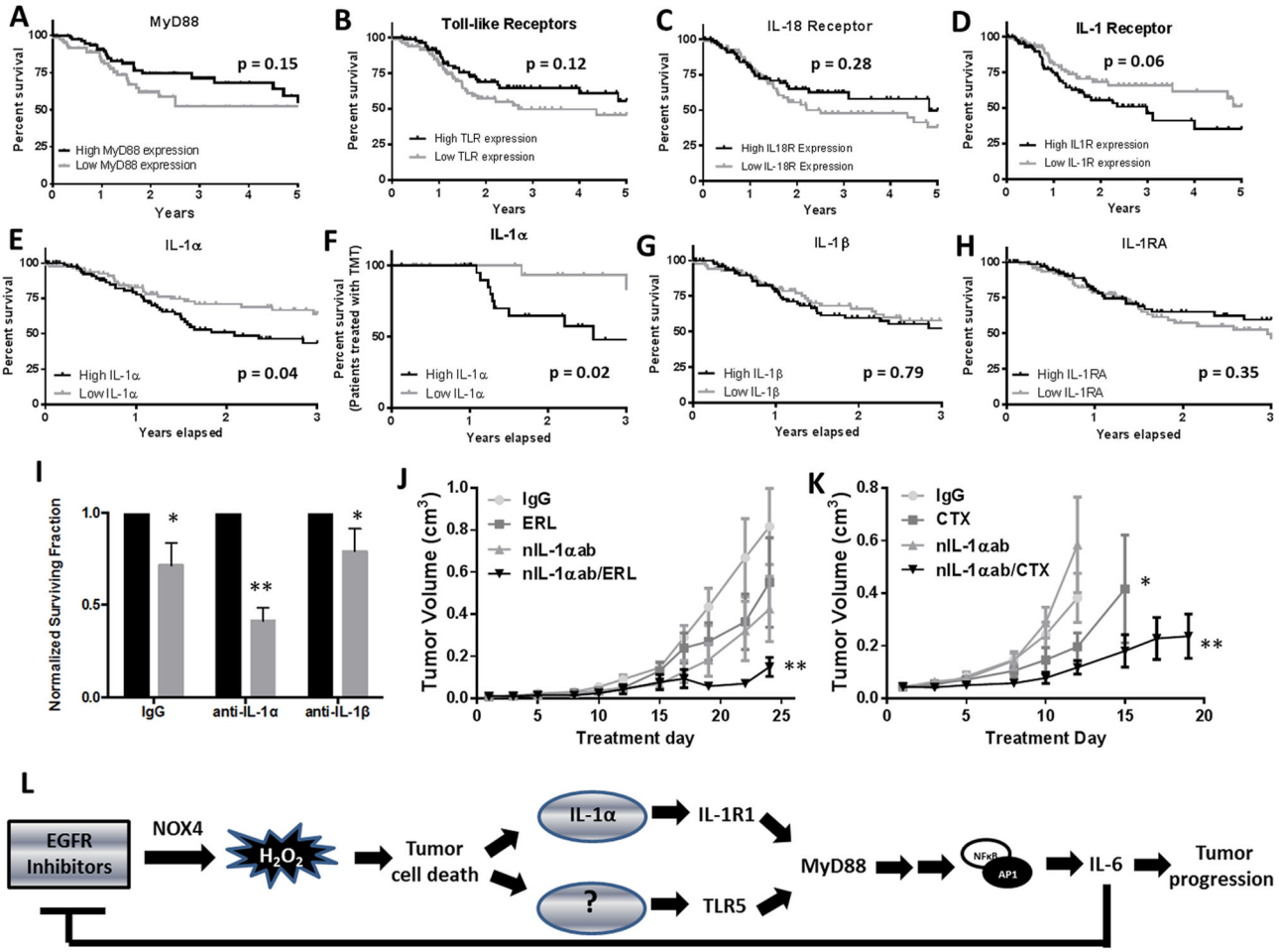

Figure 7. IL-1α expression affects response to EGFR inhibitors in HNSCC

A dataset (N=88) of HNSCC tumors from The Cancer Genome Atlas was analyzed for MyD88 (A), TLRs (B), IL-18R (C), IL-1R (D), IL-1α (E), IL-1β (G) and IL-1RN (H) expression. A dataset (N=48) of HNSCC tumors from patients that received targeted molecular therapy (TMT) was also analyzed for IL-1α expression (F). The highest quartile of expressing tumors was plotted against the lowest quartile in Kaplan-Meier survival curves. SQ20B cells were treated with IL-1α (anti-IL-1α) or IL-1β (anti-IL-1β) neutralizing antibodies for two hours prior to treatment with DMSO (black bars) or erlotinib (ERL, 5 uM, gray bars) for 48 hours then analyzed for clonogenic survival, n=3 (I). J,K: Athymic (nu/nu) mice bearing SQ20B xenograft tumors were treated as described in the Methods section. Data points represent the average tumor volume values for 10–11 mice (J,K). L: Schematic representing the proposed role of IL-1 signaling in the reduced effect of ERL in HNSCC. Error bars represent the standard error of the mean (SEM). *p<0.05 versus control; **p<0.05 versus ERL.